Magnetospheric ULF waves with increasing amplitude related to solar wind dynamic pressure changes: THEMIS observations

X.C. Shen[1,2,3], Q.-G. Zong[3], Q.Q. Shi[1], A.M. Tian[1], W.J. Sun[3], Y.F. Wang[3], X.Z. Zhou[3], S.Y. Fu[3], M.D. Hartinger[4] and V. Angelopoulos[5]

Corresponding author: Q.Q. Shi, Shandong University, Weihai, China. (sqq@sdu.edu.cn)

1Shandong Provincial Key Laboratory of Optical Astronomy and Solar-Terrestrial Environment, School of Space Science and Physics, Shandong University, Weihai, China.
3School of Earth and Space Sciences, Peking University, Beijing, China.
5Earth and Space Sciences Department, University of California, LosAngeles, California, USA.
4Atmospheric, Oceanic, and Space Sciences Department, University of Michigan, Ann Arbor, Michigan, USA.
2State Key Laboratory of Space Weather, Center for Space Science and Applied Research, Chinese Academy of Sciences, Beijing, China.

Abstract.
Ultra-low frequency (ULF) waves play an important role in transferring energy by buffeting the magnetosphere with solar wind pressure impulses. The amplitudes of magnetospheric ULF waves, which are induced by solar wind dynamic pressure enhancements or shocks, are thought to damp in one half a wave cycle or an entire wave cycle. We report in situ observations of solar wind dynamic pressure impulse-induced magnetospheric ULF waves with increasing amplitudes. We found six ULF wave events induced by solar wind dynamic pressure enhancements with slow but clear wave amplitude increase. During three or four wave cycles, the amplitudes of ion velocities and electric field of these waves increased continuously by 1.3 – 4.4 times. Two significant events were selected to further study the characteristics of these ULF waves. We found that the wave amplitude growth is mainly contributed by the toroidal mode wave. Three possible mechanisms of causing the wave amplitude increase are discussed. Firstly, solar wind dynamic pressure perturbations, which are observed in a duration of 20 – 30 minutes, might transfer energy to the magnetospheric ULF waves continually. Secondly, the wave amplitude increase in the radial electric field may becaused by superposition of two wave modes, a standing wave excited by the solar wind dynamic impulse and a propagating compressional wave directly induced by solar wind oscillations. When superposed, the two wave modes fit observations as does a calculation that superposes electric fields from two wave sources. Thirdly, the normal of the solar wind discontinuity is at an angle to the Sun-Earth line. Thus, the discontinuity will affect the dayside magnetopause continuously for a long time.

1. Introduction

[15] divided ultra low frequency (ULF) waves into several categories, including Pi waves for

irregular oscillations lasting a few wave periods and Pc waves for quasi-sinusoidal oscillations lasting relatively longer. In recent years, the important roles of these wave in the magnetosphere has been uncovered. They are, for example, thought to modulate the dynamics of energetic particles [43,3,54], contribute to electron dropout in the outer radiation belt [22,50], and excite auroral activity [10,34].

Although mechanisms that excite magnetospheric ULF waves have been studied for many years, no consensus regarding them has been reached. Early results show that the Kelvin-Helmholtz instability [29] on the magnetopause could transfer energy into the magnetosphere and excite field line resonance [14,30,8]. Some works show that a solar wind dynamic pressure impulse may excite ULF waves in the magnetosphere [48,54,52,39]. [17,18] proposed that quasi-monochromatic pulsations in the solar wind (rather than pulses) could directly drive magnetospheric pulsations. These waves could also be induced by internal processes, such as substorms tep [e.g.,][]olson1999,hsu2007,hao2014 or drift-bounce resonance with ring current ions [42].

Ultra low frequency waves in the magnetosphere are classified as toroidal mode or poloidal mode, according to the direction of magnetic field perturbations. Toroidal mode waves have a magnetic field that oscillates azimuthally; poloidal mode waves have a magnetic field that oscillates radially [45].

Although most ULF waves have been observed in the dayside magnetosphere [16,27,51,4,6,53,37,47,12], [49] observed a ULF wave driven by the cavity/waveguide modes in the magnetotail. [39] reported ULF waves induced by sudden impulses (SIs) in the nightside magnetosphere, and they propose that these waves are closely related to vortices. Recently they reported the first in situ observation of vortices induced by an increase in solar wind pressure [40].

The time evolution of nightside ULF wave activity is highly variable. Which factors contribute most strongly to this variability is unknown, but wave damping is likely one of the most important. Ultra low frequency wave energy could decay via several mechanisms, two of which are considered as critical energy sinks. One is Joule dissipation in the ionosphere for standing Alfvén waves [10]; the other is Landau damping, which transfers wave energy to particles [20]. In addition, wave energy can leak out of the magnetosphere via the magnetopause [23] or magnetotail [33]. Thus, after generation almost all reported ULF waves have decreasing wave amplitudes (e.g., [54,39,35]). Previous three-dimensional simulations of magnetosphere MHD waves driven by sudden impulses [21,7] show that single field-line resonance could result in slow rise at off-equator regions.

In this article, however, we will study waves with increasing amplitudes near the equatorial plane using in situ observations to better understand the factors affecting the time evolution of nightside ULF wave activity. In section 2, we will briefly illustrate the data sources. Section 3 shows the observations and analysis of two events. The last section will be discussion and summary.

2. Data Set

In this study, we use data from the Time History of Events and Macro-scale Interactions During Substorms (THEMIS) mission [1], which consists of five identical probes (THA, THB, THC, THD, and THE). Each probe is equipped with a fluxgate magnetometer (FGM)

[2] , which provides magnetic field data; an electrostatic analyzer (ESA) [25], which provides thermal (5 eV to 25 keV) ion and electron data; and an electric field instrument (EFI) [5], which provides 2-D electric field in the spin-plane. We use 3-s resolution spin-fit data from those instruments. Data from THEMIS ground-based observatories are also used [26]. Interplanetary magnetic field (IMF) and plasma data, which are time-shifted to the Earth's bow shock nose, are from OMNI [19].

3. Observations

Using IMF and solar wind plasma data obtained from OMNI, we reviewed solar wind dynamic pressure enhancement events from March 2007 to December 2012. The solar wind dynamic pressure enhancement is defined as an 0.5 times step-like rise in fewer than 10 seconds and stable pressure for at least 10 minutes upstream and downstream of the pressure increase front. Magnetospheric responses to these enhancements were evaluated one by one. Sixty-four ULF wave events were observed by THEMIS satellites. Of these events, six display gradual increases in amplitudes of ion velocity and electric field perturbations. The variable γ, defined as the ratio of the amplitudes (absolute value) of each half period to the first half period ($\left|\frac{A_i}{A_1}\right|$), is used to check ULF wave amplitude growth. We calculated the γ values from ion velocity and electric field data. Figure 1 shows the γ of (a) ion velocity and (b) electric field for the six events listed in Table 1 (γ_{vi-max} represents the maximum γ of the ion velocity.)

3.1. THEMIS observation

To further study ULF wave characteristics, we choose two events (the 1 April 2011 and 6 September 2012). Figure ??0 shows the locations of THA and THB during those events. During both, THB was in the solar wind and THA was on the dawn and dusk sides of the inner magnetosphere. Because THD and THE were very close to THA during both events, they observed nearly identical plasma and magnetic field variations. Similar IMF and plasma data were obtained by THB and THC, which werein the solar wind. Thus, we choose THB to monitor the solar wind variation and THA to show the magnetospheric response.

Figure 3 is an overview of (left) the 1 April 2011 (Event A) and (right) 6 September 2012 (Event B) events. All quantities in Figure 3 are in GSM coordinates. Figure 3a and Figure 3bshow the IMF and the solar wind dynamic pressure from THB. The observations of THB were time-shifted by $827s$ for Event A and $-320s$ for Event B according to the propagation speeds of the shocks and the separations between THB and THA. The shocks were identified by sharp (>1.2 nPa within 5 seconds) dynamic pressure increases and also by directional change in the magnetic field, which is marked by the red vertical dashed lines. The magnetic latitude, local time and L-shell information of THA are labeled on the bottom of Figure 3. For both events, the variations of L values of THA were lower than 0.5 Re during the time interval concerned. Therefore, the frequency variation of the field lines observed by the THA should also be limited. In addition, the magnetic latitudes of THA were lower than 10 deg from the equator, which indicates that the satellites may be located near the wave node of the field line fundamental oscillation. THEMIS-A was located in thenorthern hemisphere for

both events.

The third to the bottom panels show THA observations of (c) magnetic field components, (d) ion density, (e) total ion velocity, (f) ion velocity components, and (g) ion temperature components, respectively. Figure 3f1 and Figure 3f2 show that a clear ULF wave was excited with the arrival of interplanetary dynamic pressure enhancements for both events. More interestingly, the amplitudes of ion velocities continued increasing during three or four wave cycles. Note that the period of density fluctuation matches that of Vx for Event A, whereas the period of density fluctuation does not match that of Vx for Event B. From wavelet analysis (not shown), two typical frequencies, ⊔ 2 *mHz* and ⊔ 4 tmHz, were captured. The ⊔ 4 *mHz* density fluctuation in this event may be caused by acceleration of cold particles [32], which is consistent with the fluctuation in total velocity shown in Figure 3(e2). In addition, the density fluctuation has a wave frequency of around ⊔ 2 *mHz*, which is associated with compressional waves.

Figure 4 shows the solar wind dynamic pressure (Psw) and the wavelet analysis of Psw for both events. In addition to the sharp increases in Psw, significant wave signatures, with a frequency of ⊔ 2 *mHz*, were observed.

We performed a wavelet transform on the electric field (calculated by Vi cross B) to find the precise ULF wave frequency (shown in Figure 5). For Event A, the frequency of wave power in all three components ranges from 1.9 to 2.7*mHz* (shown in Figure 5b1 ⊔ Figure 5d1), which is in the Pc5 range. For Event B, the typical frequency is clear from 1.8 to 2.5*mHz* (shown in Figure 5b2 ⊔ Figure 5d2), also in the Pc5 range. The typical frequency bands of the two events are marked in the last three panels. For both events, after the waves were induced, the wave power between the typical frequency bands enhanced rapidly and remained high for more than half an hour.

In Figure 6, we adopted the field-aligned coordinate (FAC) system [46,12]. In that system, *r* points approximately radially outward; *a* points azimuthally eastward; and *p* is along thebackground magnetic field direction, which is obtained from the 15-min sliding averaged magnetic field. The band-pass-filtered magnetic field (blue lines in Figure 6a ⊔ Figure 6c) and electric field (red lines in Figure 6a ⊔ Figure 6c) were projected onto the FAC system. The frequency bands used in this wave mode analysis are the same bands indicated by the horizontal dashed lines in Figure 5(those corresponding to power enhancements).

Figure 6a shows perturbations in E_a and the compressional component B_p, which are typically associated with fast-mode waves. Perturbations in E_r and B_a, which are associated with toroidal modes, are presentedin Figure 6b. Figure 6c shows perturbations in E_a and B_r, which are associated with poloidal modes. In Event A, both the amplitudes of poloidal mode and toroidal mode waves are growing. In EventB, the amplitude of toroidal mode wave is increasing as that of the poloidal mode wave is decreasing. Moreover, the amplitude of the poloidal mode wave is much smaller than that of the toroidal mode wave in Event B. Figure 6d illustrates the E-B phase differences of toroidal mode (black lines) and poloidal mode (blue lines) waves. The phase differences are calculated for the waves with typical frequencies, 2.3 mHz for Event A and 2.2 mHz for Event B. After a dynamic pressure impulse arrived at the magnetosphere, the phase differences for toroidal mode waves (black lines) were around 90°, which is consistent with a standing wave signature, whereas the poloidal mode waves (blue lines) were not standing in bothevents.

3.2. Ground-based observation

Figure 7 shows the magnetic field H components from geomagnetic stations located near the magnetic latitude (MLAT) of the satellite footprints for both events. For Event A, magnetic field H components are obtained from the KAKO, INUV, SNAP, RANK, and KUUJ ground stations, respectively (their locations are labelled on each figure panel). Clear ULF wave signatures were captured by these stations. The main frequency is consistent with that from the THEMIS observations. The data are band-pass filtered from 1.9 mHz to 2.7 mHz, which shows that magnetic field H component wave amplitude increases 2.4 to 4.1 times after wave induction. The clear wave amplitude increase was observed in large longitudinal regions from geomagnetic longitude 264.9suremath

34 (thelongitudinalseparati1018

Ground-based magnetic field data were further used to calculate the wave number for Event A. We know the wave number $m = \delta\varphi / \delta\lambda$ [36], where $\delta\varphi$ represents the phase difference of the H magnetic field componentand $\delta\lambda$ is the azimuthal separation (*i.e.*, longitudinal difference) between the two stations. When calculating the wave number, even a small separation in geomagnetic latitude between two stations may result in considerable error citepsarris2013. To minimize error, we choose stations with small differences in geomagnetic latitudes (fewer than 0.5°; see Table 2). The geomagnetic longitude and latitude of the footprint of THA at 16:00 UT were 188.9° and 71.3°, respectively. First, we choose two close stations, KAKO and INUV, with azimuthal separation $\delta\lambda$ = 10.92. Figure 8 (left) shows ground-based observations ofwaves from a pair of ground stations located near the footprint of THA in Event A. Figure 8a1 and Figure 8b1 show the wavelet power spectra of magnetic field H components of two stations, and the H components of magnetic fields are overplotted. Both stations captured significant wave signatures. The typical frequency is around $2.5mHz$ for both stations.The squared wavelet coherence between magnetic field H components of two stations is shown in Figure 8c1. The black solid lines in Figure 8a □ Figure 8c mark the main frequency $2.5mHz$ used to calculate the phase difference, as shown in Figure 8d1. The green, black and red lines show the phase differences between waves in 2.4, 2.5 and $2.7mHz$ in Figure 8d1. The phase differences tend to be stable between 16:28 (UT) and 16:50 (UT). We obtain the phase difference as □ $(360n + 45)^\circ$ around 16:30 (UT). Using the same method, one more phase difference is calculated as □ $(360n' + 170)^\circ$ from another pair of stations, KAKO and SNAP, with larger separation in the azimuthal direction ($\delta\lambda$ = 41.93; see the righthand plot of Figure 8). The ratio of these two phase differences and the ratio of two longitudinal differences of two pairs of stations should be equal. Thus, n and n' are calculated as 0. Given that the magnetic longitude difference between the two stations is 10.92° (shown in Table 2), for the first pair of stations the wave number is calculated as ≈ 4.12. Similarly, for the second pair of stations, the wave number is ≈ 4.05 (shown in Table 2). The small wave number indicates that the standing toroidal wave may be driven by a waveguide mode (e.g., [14]). For Event B, the stations located near the footprint of THA (GeoM: Lon. 12.0°, Lat. 72.2°) did not provide high time resolution magnetic field

data. Thus, the wavenumber for Event B was not calculated.

4. Discussion

The amplitudes of magnetospheric ULF waves, which are induced by solar wind dynamic pressure enhancements or shocks, are thought to damp rapidly. However, in the six Pc5 wave events we observed, the wave amplitudes of ion velocities and electric fields could increase gradually by more than four times during three or four cycles.

4.1. Solar wind discontinuity normal direction

An amplitude increase may occur because the normal of the solar wind discontinuity is at an angle to the Sun-Earth line. Thus, the discontinuity will affect the dayside magnetopause continuously for a long time. Interaction between the discontinuity andthe magnetosphere at various locations and at various times may cause compressional waves to be launched, and superposition of these waves may result in a slow increase in toroidal wave amplitude. We calculated the normal directions of solar winddiscontinuities for the two events using the Timing method [31]. They are [-0.90, -0.41, -0.10] (calculated from CLUSTER four satellites) and [-0.94, 0.13, 0.31] (calculated from THEMIS-B, C, WIND and ACE satellites), respectively. The angle between the normal direction of the solar wind discontinuity and the Sun-Earth line is about 26 degrees for Event A and 20 degrees for Event B. The velocities of the discontinuities, obtained from Timing method, are 330 km/s for Event A and 484 km/s for Event B. However, these angles are not large enough to produce a gradual increase in wave amplitude for nearly half an hour in the two events.

4.2. Solar wind dynamic pressure perturbations

Wave signatures with frequencies around 2 *mHz* were captured in solar wind dynamic pressures for both events (see Figure 4). The wave power in the second panel of Figure 4 shows that both Psw oscillations inthe two events lasted for almost half an hour. Compressional waves, which could be induced by the Psw oscillations [17,18], continuously couple to the standing toroidal mode wave for about half an hour. Furthermore, the time scales of wave amplitude increases shown in Figure 3 are between 20 and 30 minutes. Thus, we suggest that one wave energy input could be Psw perturbation.

4.3. Wave mode superposition

The wave energy peaks in Psw are 2.1 *mHz* and 2.0 *mHz* at 16:24 UT and 16:44 UT (without time shift) for the two events, respectively (see Figure 4), and the frequencies of the toroidal mode waves are 2.4 tmHz and 2.3 *mHz* (shown in Figure 9b). Even though the frequencies of Psw oscillations are extremely close to that of the magnetic field azimuthal component observed in the magnetosphere, a small difference between them still exists. Therefore, another scenario, superposition of two wave modes, is discussed. One wave mode is a standing wave excited by a sharp solar wind dynamic impulse, as shown in Figure 6b. The magnetic field lines are continuously shaken by traveling, compressional waves, as indicated by continuous oscillations in the magnetic field p component (i.e., along the magnetic field

line) (shown in Figure 9c). [17,18] proposed that thepressure balance between the inside and the outside of the magnetosphere could cause magnetospheric ULF waves to be directly excited by solar wind dynamic pressure perturbations. Significant wave power around □ 2 *mHz* was observed inthe solar wind dynamic pressure for the two events (see Figure 4). Thus, the traveling compressional wave in both events might be directly driven by solar wind dynamic pressure perturbations, and the compressional wave frequency mightbe controlled by the frequency of the solar wind dynamic pressure perturbations [18]. The electric field of the standing wave oscillates radially, and the electric field of the compressional wave oscillates radially and azimuthally. Thus, electric fields of two wave sources may superpose in the radial direction. We calculate the superposition of two waves for two events. The functions of the two wave sources are as follows:

$\psi_1 = A_1 \cos(\phi_1 - \omega_1 t)$ (1) $\psi_2 = A_2 \cos(\phi_2 - \omega_2 t)$ (2)

After superposing these two waves, the wave function changes to:

$\psi_{superposed} = \psi_1 + \psi_2 = A_1 \cos(\phi_1 - \omega_1 t) + A_2 \cos(\phi_2 - \omega_2 t)$ (3)

If two wave sources with very close frequencies and amplitudes are superposed on a wave, the amplitude of that wave will vary from a minimum to a maximum value. This type of wave is called a beat wave. We used the same amplitude for two waves in the calculation (i.e. $A_1 = A_2 = A_0$). The decay effect has also been considered. The filtered Er component in Figure 6 shows that wave signatures are observed during one hour. We consider the wave amplitude decrease to 1/e times the initial amplitude in one hour. Thus, the decay factor is $e^{-\frac{t}{3600}}$.

Therefore, the superposed wave in our calculation was modified as follows:

$\psi_{superposed} = \psi_1 + \psi_2 = 2A_0 e^{-\frac{t}{3600}} \cos(\frac{(\phi_1+\phi_2)-(\omega_1+\omega_2)t}{2}) \cos(\frac{(\phi_1-\phi_2)-(\omega_1-\omega_2)t}{2})$ (4)

In the calculation, the frequencies for two wave sources are determined by wavelet analyses of Ba and Bp (shown in Figure 9), because Ba is associated with a toroidal mode wave and Bp is associated with a compressional wave. For Event A, $\omega_1 = 2.4mHz$ and $\omega_2 = 2.1mHz$; for Event B, $\omega_1 = 2.3mHz$ and $\omega_2 = 1.9mHz$. The phases of the waves are defined to match the observed beat wave. For Event A, $A_0 = 3.5$, $\phi_1 = -\frac{1}{2}\pi$), $\phi_2 = -\frac{5}{4}\pi$; for Event B, $A_0 = 1.7$, $\phi_1 = -\frac{1}{2}\pi$, $\phi_2 = -\frac{3}{2}\pi$.

Figure 10b shows the superposition of these two wave sources. In these two events, the timescale of wave amplitude increase and decrease in the calculation matches the observations fairly well. Almost half an hour and three periods were required to reach maximum wave amplitude. The waves damp within the next half an hour and three periods. Therefore, the wave amplitude increase could be caused by superposition of two wave sources.

5. Summary

Previous observations show that after induction most magnetospheric ULF waves decrease in

wave amplitude. By checking the responses of the magnetosphere to dynamic pressure enhancements from 1 April 2007 to 31 December 2012, we found six ULF waves with slow but clear wave amplitude increase.

Two significant events were chosen to further study the characteristics of these ULF waves. Both events show that the wave amplitude increases were mostly contributed by toroidal mode standing waves. Three wave amplitude increase mechanisms are discussed.First, because the normal of the solar wind discontinuity is at an angle to the Sun-Earth line, the discontinuity will affect the dayside magnetopause continuously for a long time. Second, solar wind dynamic pressure perturbations, observed for 20 □ 30 minutes, could continuously transfer energy to magnetospheric ULF waves. Third, two wave modes, a standing wave excited by the solar wind dynamic impulse and a propagating compressional wave directly induced by solar wind oscillations, could superimpose, causing a wave amplitude increase in the radial electric field.

Our main conclusions are summarized below:

1. We found six ULF waves with slow but clear wave amplitude increase. The amplitudes of ion velocities and electric field of these waves increased continuously by a factor of 1.3 □ 4.4 during three to four wave cycles.
2. According to our case studies of Events A and B, the wave amplitude increases were mostly contributed by toroidal mode standing waves.
3. Three factors, (1) normal direction of solar wind discontinuities, (2) solar wind dynamic pressure perturbations, and (3) wave mode superposition, could contribute to these increases.
4. Wave mode superposition could be responsible for the wave amplitude increases in Event A and B.

We acknowledge NASA contract NAS5-02099 and V. Angelopoulos for use of data from the THEMIS Mission (http://themis.ssl.berkeley.edu/data/themis/). Specifically: J. W. Bonnell and F. S. Mozer for use of EFI data, C. W. Carlson and J. P. McFadden for use of ESA data, K. H. Glassmeier, U. Auster and W. Baumjohann for the use of FGM data provided under the lead of the Technical University of Braunschweig and with financial support through the German Ministry for Economy and Technology and the German Center for Aviation and Space (DLR) under contract 50 OC 0302, S. Mende and C. T. Russell for use of the GMAG data and NSF for support through grant AGS-1004814 and data provided by the Geophysical Institute Magnetometer Array operated by theGeophysical Institute, University of Alaska. We also acknowledge use of OMNI data obtained from NASA/GSFC's Space Physics Data Facility's OMNIWeb service at http://omniweb.gsfc.nasa.gov. This work is supported by the National Natural Science Foundation of China (Grant Nos. 41322031, 41031065, 41404131), the Specialized Research Fund for State Key Laboratories, the scientific research foundation of Shandong province Outstanding Young Scientist Award (Grant No. 2013BSE27132), the Shandong Natural Science Foundation JQ201112, and the Ministry of Education of China (NCET-12-0332). We thank Judith Hohl for help with editing.

[1] Angelopoulos, V. (2008), The THEMIS mission, *Space Science Reviews*, *141*, doi:10.1007/s11214-008-9336-1.

[2] Auster, H. U., K. H. Glassmeier, W. Magnes, O. Aydogar, W. Baumjohann, D. Constantinescu, D. Fischer, K. H. Fornacon, E. Georgescu, P. Harvey, O. Hillenmaier, R. Kroth, M. Ludlam, Y. Narita, R. Nakamura, K. Okrafka, F. Plaschke, I. Richter,

H. Schwarzl, B. Stoll, A. Valavanoglou, and M. Wiedemann (2008), The THEMIS fluxgate magnetometer, *Space Science Reviews*, *141*, doi:10.1007/s11214-008-9365-9.
[3] Baumjohann, W., O. H. Bauer, G. Haerendel, H. Junginger, and E. Amata (1983), Magnetospheric plasma drifts during a sudden impulse, *Journal of Geophysical Research*, doi:10.1029/JA088iA11p09287.
[4] Baumjohann, W., H. Junginger, G. Haerendel, and O. H. Bauer (1984), Resonant alfvén waves excited by a sudden impulse, *Journal of Geophysical Research*, doi:10.1029/JA089iA05p02765.
[5] Bonnell, J., F. Mozer, G. Delory, A. Hull, R. Ergun, C. Cully, V. Angelopoulos, and P. Harvey (2008), The electric field instrument (efi) for themis, *Space Science Reviews*, *141*(1-4), 303–341.
[6] Cahill, L. J., N. G. Lin, J. H. Waite, M. J. Engebretson, and M. Sugiura (1990), Toroidal standing waves excited by a storm sudden commencement: DE 1 observations, *Journal of Geophysical Research*, doi:10.1029/JA095iA06p07857.
[7] Chi, P. J., D. -H. Lee, and C. T. Russell (2006), Tamao travel time of sudden impulses and its relationship to ionospheric convection vortices, *Journal of Geophysical Research*, doi:10.1029/2005JA011578.
[8] Claudepierre, S. G., S. R. Elkington, and M. Wiltberger (2008), Solar wind driving of magnetospheric ULF waves: Pulsations driven by velocity shear at the magnetopause, *Journal of Geophysical Research*, *113*, doi:10.1029/2007JA012890.
[9] Cummings, W. D., R. J. O'Sullivan, and P. J. Coleman Jr. (1969), Standing AlfvÃ©n waves in the magnetosphere, *Journal of Geophysical Research*, doi:10.1029/JA074i003p00778.
[10] Greenwald, R. A., and A. D. M. Walker (1980), Energetics of long period resonant hydromagnetic waves, *Geophysical Research Letters*, doi:10.1029/GL007i010p00745.
[11] Hao, Y. X., Q. Zong, Y. F. Wang, X. Zhou, H. Zhang, S. Y. Fu, Z. Y. Pu, H. E. Spence, J. B. Blake, J. Bonnell, J. R. Wygant, and C. A. Kletzing (2014), Interactions of energetic electrons with ULF waves triggered by interplanetary shock: Van allen probes observations in the magnetotail, *Journal of Geophysical Research: Space Physics*, doi:10.1002/2014JA020023.
[12] Hartinger, M., V. Angelopoulos, M. B. Moldwin, K. Glassmeier, and Y. Nishimura (2011), Global energy transfer during a magnetospheric field line resonance, *Geophysical Research Letters*, *38*, doi:10.1029/2011GL047846.
[13] Hsu, T., and R. L. McPherron (2007), A statistical study of the relation of pi 2 and plasma flows in the tail, *Journal of Geophysical Research*, *112*, doi:10.1029/2006JA011782.
[14] Hudson, M. K., R. E. Denton, M. R. Lessard, E. G. Miftakhova, and R. R. Anderson (2004), A study of pc-5 ULF oscillations, *Annales Geophysicae*, *22*, doi:10.5194/angeo-22-289-2004.
[15] Jacobs, J. A., Y. Kato, S. Matsushita, and V. A. Troitskaya (1964), Classification of geomagnetic micropulsations, *Geophysical Journal of the Royal Astronomical Society*, *8*, doi:10.1111/j.1365-246X.1964.tb06301.x.
[16] Kaufmann, R. L., and D. N. Walker (1974), Hydromagnetic waves excited during an ssc, *Journal of Geophysical Research*, doi:10.1029/JA079i034p05187.
[17] Kepko, L. (2002), ULF waves in the solar wind as direct drivers of magnetospheric pulsations, *Geophysical Research Letters*, *29*, doi:10.1029/2001GL014405.

[18] Kepko, L. (2003), Observations of discrete, global magnetospheric oscillations directly driven by solar wind density variations, *Journal of Geophysical Research, 108*, doi:10.1029/2002JA009676.
[19] King, J., and N. Papitashvili (2005), Solar wind spatial scales in and comparisons of hourly wind and ace plasma and magnetic field data, *Journal of Geophysical Research: Space Physics (1978–2012), 110*(A2).
[20] Landau, L. (1946), On the vibrations of the electronic plasma, *J. Phys., 10*(25).
[21] Lee, D. -H., and M. K. Hudson(2001), Numerical studies on the propagation of sudden impulses in the dipole magnetosphere, *Journal of Geophysical Research*, doi:10.1029/2000JA000271.
[22] Loto'aniu, T. M., H. J. Singer, C. L. Waters, V. Angelopoulos, I. R. Mann, S. R. Elkington, and J. W. Bonnell (2010), Relativistic electron loss due to ultralow frequency waves and enhanced outward radial diffusion, *Journal of Geophysical Research*, doi:10.1029/2010JA015755.
[23] Mann, I. R., and A. N. Wright (1999), Diagnosing the excitation mechanisms of pc5 magnetospheric flank waveguide modes and FLRs, *Geophysical Research Letters*, doi:10.1029/1999GL900573.
[24] Mann, I. R., A. N. Wright, and P. S. Cally (1995), Coupling of magnetospheric cavity modes to field line resonances: A study of resonance widths, *Journal of Geophysical Research: Space Physics (1978?2012)*, doi:10.1029/95JA00820.
[25] McFadden, J. P., C. W. Carlson, D. Larson, M. Ludlam, R. Abiad, B. Elliott, P. Turin, M. Marckwordt, and V. Angelopoulos (2008), The THEMIS ESA plasma instrument and in-flight calibration, *Space Science Reviews*, *141*, doi:10.1007/s11214-008-9440-2.
[26] Mende, S., S. Harris, H. Frey, V. Angelopoulos, E. Donovan, B. Jackel, M. Greffen, C. Russell, and L. Peticolas (2008), A large array of ground based observatories for the study of auroral substorms, *Space Sci. Rev*.
[27] Nopper, R. W., W. J. Hughes, C. G. Maclennan, and R. L. McPherron (1982), Impulse-excited pulsations during the july 29, 1977, event, *Journal of Geophysical Research*, doi:10.1029/JA087iA08p05911.
[28] Olson, J. V. (1999), Pi2 pulsations and substorm onsets: A review, *Journal of Geophysical Research*, *104*, doi:10.1029/1999JA900086.
[29] Pu, Z., and M. G. Kivelson (1983), Kelvin:Helmholtz instability at the magnetopause: Solution for compressible plasmas, *Journal of Geophysical Research, 88*, doi:10.1029/JA088iA02p00841.
[30] Rae, I. J., E. F. Donovan, I. R. Mann, F. R. Fenrich, C. E. J. Watt, D. K. Milling, M. Lester, B. Lavraud, J. A. Wild, H. J. Singer, H. Rème, and A. Balogh (2005), Evolution and characteristics of global pc5 ULF waves during a high solar wind speed interval, *Journal of Geophysical Research*, doi:10.1029/2005JA011007.
[31] Russell, C. T., J. T. Gosling, R. D. Zwickl, and E. J. Smith (1983), Multiple spacecraft observations of interplanetary shocks: ISEE three-dimensional plasma measurements, *Journal of Geophysical Research*, doi:10.1029/JA088iA12p09941.
[32] Sakurai, T., Y. Tonegawa, T. Kitagawa, M. Nowada, A. yamawaki, T. Mukai, S. Kokubun, T. Yamamoto, and K. Tsuruda (1999), Double-frequency oscillations of low energy plasma associated with transverse Pc5 pulsations: Geotail satellite observations, tEarth Planets Space, *51* 43-53.

[33] Samson, J. C., D. D. Wallis, T. J. Hughes, F. Creutzberg, J. M. Ruohoniemi, and R. A. Greenwald (1992), Substorm intensifications and field line resonances in the nightside magnetosphere, *Journal of Geophysical Research: Space Physics (1978-2012)*, doi:10.1029/91JA03156.
[34] Samson, J. C., L. L. Cogger, and Q. Pao (1996), Observations of field line resonances, auroral arcs, and auroral vortex structures, *Journal of Geophysical Research*, doi:10.1029/96JA01086.
[35] Samsonov, A. A., D. G. Sibeck, B. M. Walsh, and N. V. Zolotova (2014), Sudden impulse observations in the dayside magnetosphere by THEMIS, *Journal of Geophysical Research: Space Physics*, doi:10.1002/2014JA020012.
[36] Sarris, T. E., W. Liu, K. Kabin, X. Li, S. R. Elkington, R. Ergun, R. Rankin, V. Angelopoulos, J. Bonnell, K. H. Glassmeier, and U. Auster (2009), Characterization of ULF pulsations by THEMIS, *Geophysical Research Letters*, *36*, doi:10.1029/2008GL036732.
[37] Sarris, T. E., W. Liu, X. Li, K. Kabin, E. R. Talaat, R. Rankin, V. Angelopoulos, J. Bonnell, and K. H. Glassmeier (2010), THEMIS observations of the spatial extent and pressure-pulse excitation of field line resonances, *Geophysical Research Letters*, doi:10.1029/2010GL044125.
[38] Sarris, T. E., X. Li, W. Liu, E. Argyriadis, A. Boudouridis, and R. Ergun (2013), Mode number calculations of ULF field-line resonances using ground magnetometers and THEMIS measurements, *Journal of Geophysical Research: Space Physics*, doi:10.1002/2012JA018307.
[39] Shi, Q. Q., M. Hartinger, V. Angelopoulos, Q. Zong, X. Zhou, X. Zhou, A. Kellerman, A. M. Tian, J. Weygand, S. Y. Fu, Z. Y. Pu, J. Raeder, Y. S. Ge, Y. F. Wang, H. Zhang, and Z. H. Yao (2013), THEMIS observations of ULF wave excitation in the nightside plasma sheet during sudden impulse events, *Journal of Geophysical Research: Space Physics*, *118*, doi:10.1029/2012JA017984.
[40] Shi, Q. Q., M. Hartinger, V. Angelopoulos, A. Tian, S. Fu, Q.-G. Zong, J. Weygand, J. Raeder, Z. Pu, X. Zhou, M. Dunlop, W. Liu, H.Zhang, Z. Yao, and X. Shen (2014), Solar wind pressure pulse?driven magnetospheric vortices and their global consequences, *Journal of Geophysical Research: Space Physics*, *119*(6), 4274–4280, doi:10.1002/2013JA019551.
[41] Shue, J., P. Song, C. T. Russell, J. T. Steinberg, J. K. Chao, G. Zastenker, O. L. Vaisberg, S. Kokubun, H. J. Singer, T. R. Detman, and H. Kawano (1998), Magnetopause location under extreme solar wind conditions, *Journal of Geophysical Research*, *103*, doi:10.1029/98JA01103.
[42] Southwood, D., J. Dungey, and R. Etherington (1969), Bounce resonant interaction between pulsations and trapped particles, *Planetary and Space Science*, *17*, doi:10.1016/0032-0633(69)90068-3.
[43] Southwood, D. J., and M. G. Kivelson (1981), Charged particle behavior in low-frequency geomagnetic pulsations 1. transverse waves, *Journal of Geophysical Research*, *86*, doi:10.1029/JA086iA07p05643.
[44] Southwood, D. J., and M. G. Kivelson (1990), The magnetohydrodynamic response of the magnetospheric cavity to changes in solar wind pressure, *Journal of Geophysical Research: Space Physics*, *95*(A3), 2301–2309, doi:10.1029/JA095iA03p02301.
[45] Sugiura, M., and C. Wilson (1964), Oscillation of the geomagnetic field lines and associated magnetic perturbations at conjugate points, *Journal of Geophysical Research:*

Space Physics, *69*(7).
[46] Takahashi, K., M. RW, A. Lui, and T. Potemra (1990), Ion flux oscillations associated with a radially polarized transverse pc 5 magnetic pulsation, *Journal of Geophysical Research: Space Physics (1978Â–2012)*, *95*(A4), 3717–3731, doi:10.1029/JA095iA04p03717.
[47] Takahashi, K., J. Bonnell, K.-H. Glassmeier, V. Angelopoulos, H. Singer, C. P.J., R. Denton, N. Y., D. Lee, M. Nosé, and W. Liu (2010), Multipoint observation of fast mode waves trapped in the dayside plasmasphere, *Journal of Geophysical Research: Space Physics (1978â€“2012)*, *115*(A12), doi:10.1029/2010JA015956.
[48] Tan, L. C. (2004), Observation of magnetospheric relativistic electrons accelerated by pc-5 ULF waves, *Geophysical Research Letters*, *31*, doi:10.1029/2004GL019459.
[49] Tian, A. M., Q. G. Zong, T. L. Zhang, R. Nakamura, A. M. Du, W. Baumjohann, K. H. Glassmeier, M. Volwerk, M. Hartinger, Y. F. Wang, J. Du, B. Yang, X. Y. Zhang, and E. Panov (2012), Dynamics of long-period ULF waves in the plasma sheet: Coordinated space and ground observations, *Journal of Geophysical Research*, *117*, doi:10.1029/2011JA016551.
[50] Turner, D. L., Y. Shprits, M. Hartinger, and V. Angelopoulos (2012), Explaining sudden losses of outer radiation belt electrons during geomagnetic storms, *Nature Physics*, doi:10.1038/nphys2185.
[51] Wilken, B., C. K. Goertz, D. N. Baker, P. R. Higbie, and T. A. Fritz (1982), The SSC on july 29, 1977 and its propagation within the magnetosphere, *Journal of Geophysical Research*, doi:10.1029/JA087iA08p05901.
[52] Zhang, X. Y., Q. Zong, Y. F. Wang, H. Zhang, L. Xie, S. Y. Fu, C. J. Yuan, C. Yue, B. Yang, and Z. Y. Pu (2010), ULF waves excited by negative/positive solar wind dynamic pressure impulses at geosynchronous orbit, *Journal of Geophysical Research*, *115*, doi:10.1029/2009JA015016.
[53] Zong, Q., X. Zhou, X. Li, P. Song, S. Y. Fu, D. N. Baker, Z. Y. Pu, T. A. Fritz, P. Daly, A. Balogh, and H. Réme (2007), Ultralow frequency modulation of energetic particles in the dayside magnetosphere, *Geophysical Research Letters*, *34*, doi:10.1029/2007GL029915.
[54] Zong, Q., X. Zhou, Y. F. Wang, X. Li, P. Song, D. N. Baker, T. A. Fritz, P. W. Daly, M. Dunlop, and A. Pedersen (2009), Energetic electron response to ULF waves induced by interplanetary shocks in the outer radiation belt, *Journal of Geophysical Research*, *114*, doi:10.1029/2009JA014393.

1. Wave amplitude increase versus wave cycle of (a) ion velocity and (b) electric field for six magnetospheric ULF wave events. Electric fields are calculated by $V_i \times B$. γ is defined as the amplitude of each half wave period divided by the amplitude of the first half wave period. Crosses represent calculated γ.

Dashed lines are linear fitting of the crosses. Different colors represent different events.

2. The locations of THA and THB for two events. The purple symbols are for the 1 April 2011 event (Event A), and the blue symbols are for the 6 September 2012 event. The curved black line indicates the location of the magnetopause which is calculated from the [41] model using the solar wind dynamic pressure $D_p = 2.0nPa$ and $B_z = 1.0nT$.

3. Overview of two events from (left) 16:15 to 17:15 UT on 1 April 2011 (Event A) and (right) 16:30 to 17:30 UT on 6 September 2012 (Event B). From top to bottom, the panels show (a) IMF, (b) solar wind dynamic pressure, (c) magnetospheric magnetic field components, (d) ion density, (e) total ion velocity, (f) ion velocity and (g) ion temperature, respectively. The solar wind and IMF data are time shifted as labeled in the panels. The red vertical dashed lines indicate the sudden enhancements of the solar wind dynamic pressure.

4. The (a) solar wind dynamic pressure fluctuations and (b) their wavelet analyses for (left) Event A and (right) Event B.

5. Wavelet analysis of the electric field (obtained from Vi cross B) for (left) Event A (1 April 2011) and (right) Event B (6 September 2012). From top to bottom, the panels show (a) three components of the electric field in GSM coordinates and the wavelet analysis of (b) the x, (c) y, and (d) z components, respectively, of the electric field. The dashed lines in the last three panels mark the strongest frequency bands. For Event A, the frequency of wave power in all three components ranges from 1.9 to $2.7mHz$. For Event B, the typical frequency is clear from 1.8 to $2.5mHz$. The red vertical dashed lines indicate the sudden enhancements in the solar wind dynamic pressure.

6. Magnetic and electric fields in field-aligned coordinates (FAC) and phase differences between their components for (left) Event A and (right) Event B. From top to bottom, the panels show (a) Bp-Ea, (b) Ba-Er, (c) Br-Ea and (d) phase difference between the magnetic and electric fields. The data have been band-pass filtered in the range of 1.9 to 2.7 mHz for Event A and 1.8 to 2.5 mHz for Event B. The black dashed lines in the panel d mark the $\pm 90^\circ$. Note that in both events, the waves are standing in toroidal mode but propagating in poloidal mode. The red vertical dashed lines indicate the sudden enhancements in the solar wind dynamic pressure.

7. Magnetic field H components from GMAG stations for Event A (left) and Event B (right). Blue dashed line indicates the magnetic field H component and black solid line indicates the filtered magnetic field H component. For Event A, the data are filtered from 1.9 mHz to 2.7 mHz; for Event B, the data are filtered from 1.8 to 2.5 mHz.

8. Magnetic field H components from GMAG stations and their phase differences for Event A. Panel a and b show the wavelet analysis of the magnetic field H component. Magnetic field H component data are overplotted on each panel. Panel c illustrates the squared wavelet coherence between magnetic field H components from two stations. The white solid lines in panel a □ c mark the frequency of $2.5mHz$, which is used to calculate the phase difference between two H components (shownin the last panel). The red vertical dashed lines indicate the sudden enhancements in the solar wind dynamic pressure.

9. The parallel and azimuthal magnetic field components and their wavelet analyses for (left) Event A and (right) Event B. From top to bottom, the panels show (a) B_a, (b) wavelet analysis of B_a, (c) B_p and (d) wavelet analysis of B_p. The typical frequencies for B_a and B_p are marked by dashed white lines and the values are labelled above the lines.

10. The observed and simulated Er for (left) Event A and (right) Event B. From top to bottom are (a) the *radial* component of the unfiltered electric field in the FAC system from 16:20 to 17:20 UT observed by THA and (b) the *radial* component of the electric field calculated by superposition of two wave sources. In panel b, the blue and green dashed lines indicate two wave sources and the black solid lines illustrate the superposed waves.

1. THEMIS observations of wave amplitude increases

No.	Time (yyyy/mm/dd)	Locations (GSM: x, y, z)	MLat (deg)	γ_{Vi-max}	Increasing periods
1	2009/11/08	(3.0, -6.9, -0.8)	-5.9	1.6	3
2	2009/12/25	(-1.8, -8.9, -1.2)	-7.7	1.3	3
3	2011/04/01	(-6.3, -8.4, 1.6)	8.8	4.0	3
4	2011/09/10	(-0.4, 10.3, 0.0)	0.1	2.1	4
5	2012/05/08	(-3.8, -8.3, 0.5)	3.2	2.6	4
6	2012/09/06	(-0.5, 8.9, 0.5)	3.5	4.4	4

2. Wave numbers calculated from the ground station observations

Date	Station 1 (Geom: Lat, Long)	Station 2 (Geom: Lat, Long)	$\delta\varphi(^\circ)$	$\delta\lambda(^\circ)$	m
2011/04/01	KAKO (71.1, 264.8)	INUV (71.2, 275.8)	≈ 45	10.92	≈ 4.12
2011/04/01	KAKO (71.1, 264.8)	SNAP (70.8, 306.8)	≈ 170	41.93	≈ 4.05

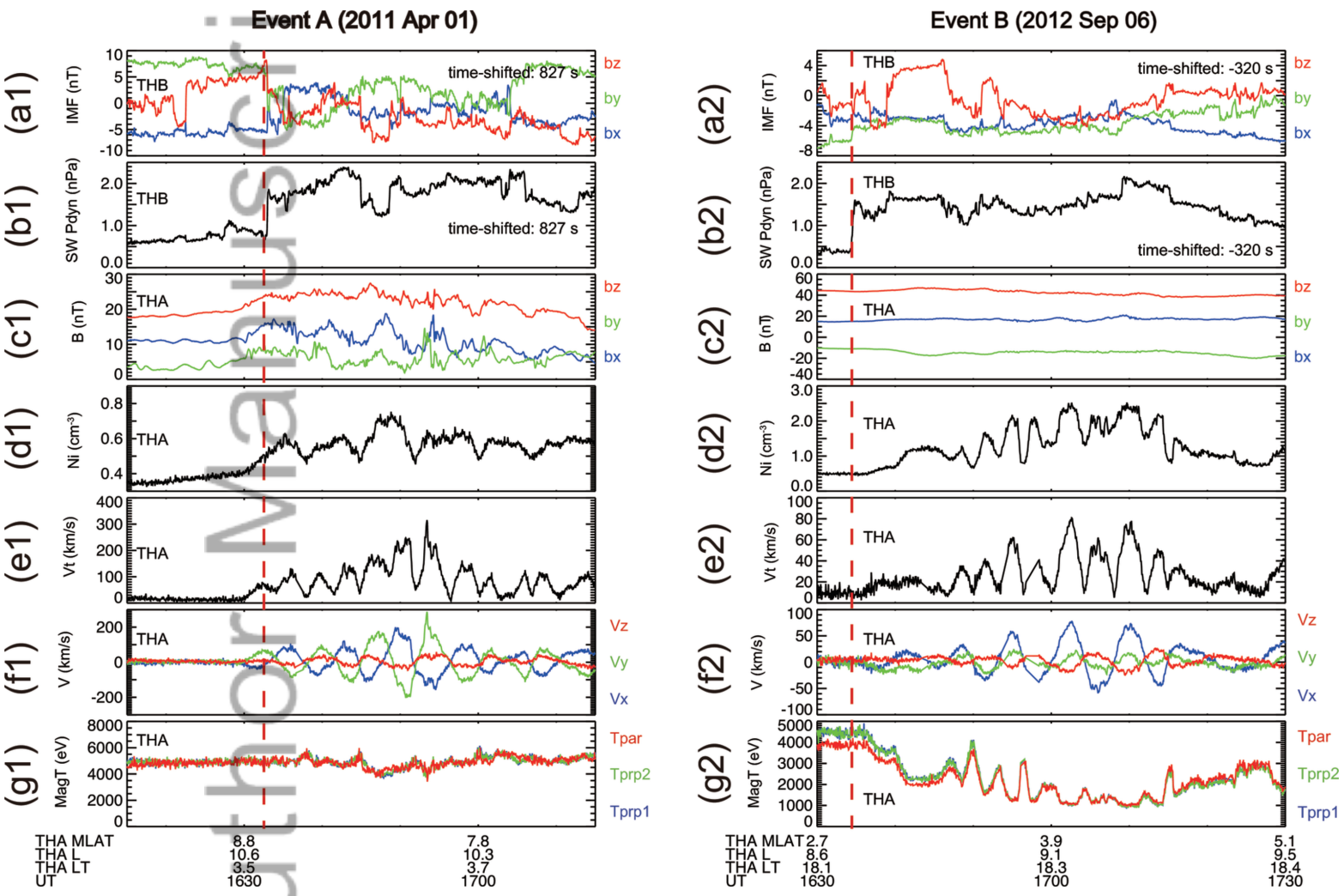

combinecase

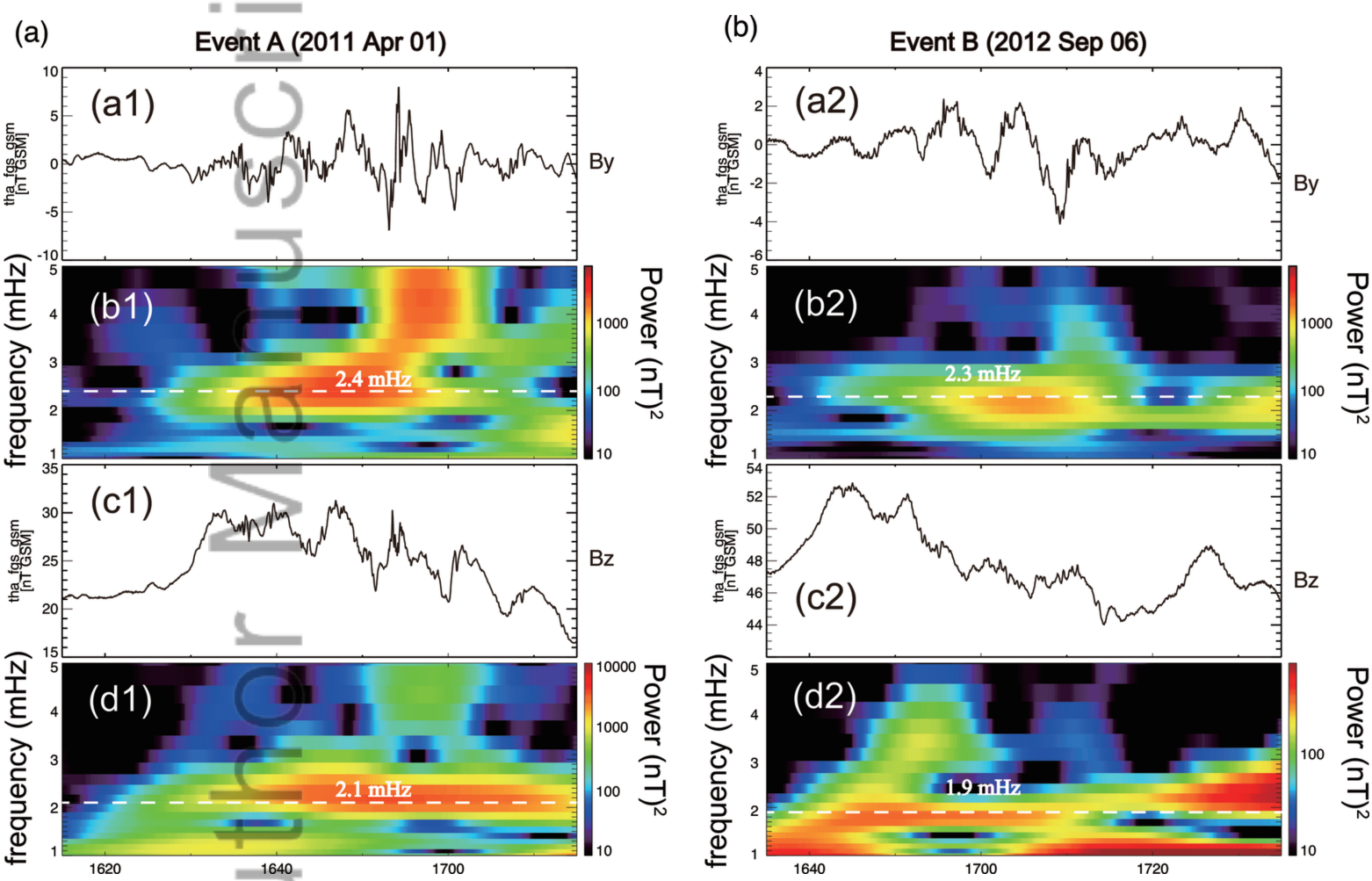

frequencychoose

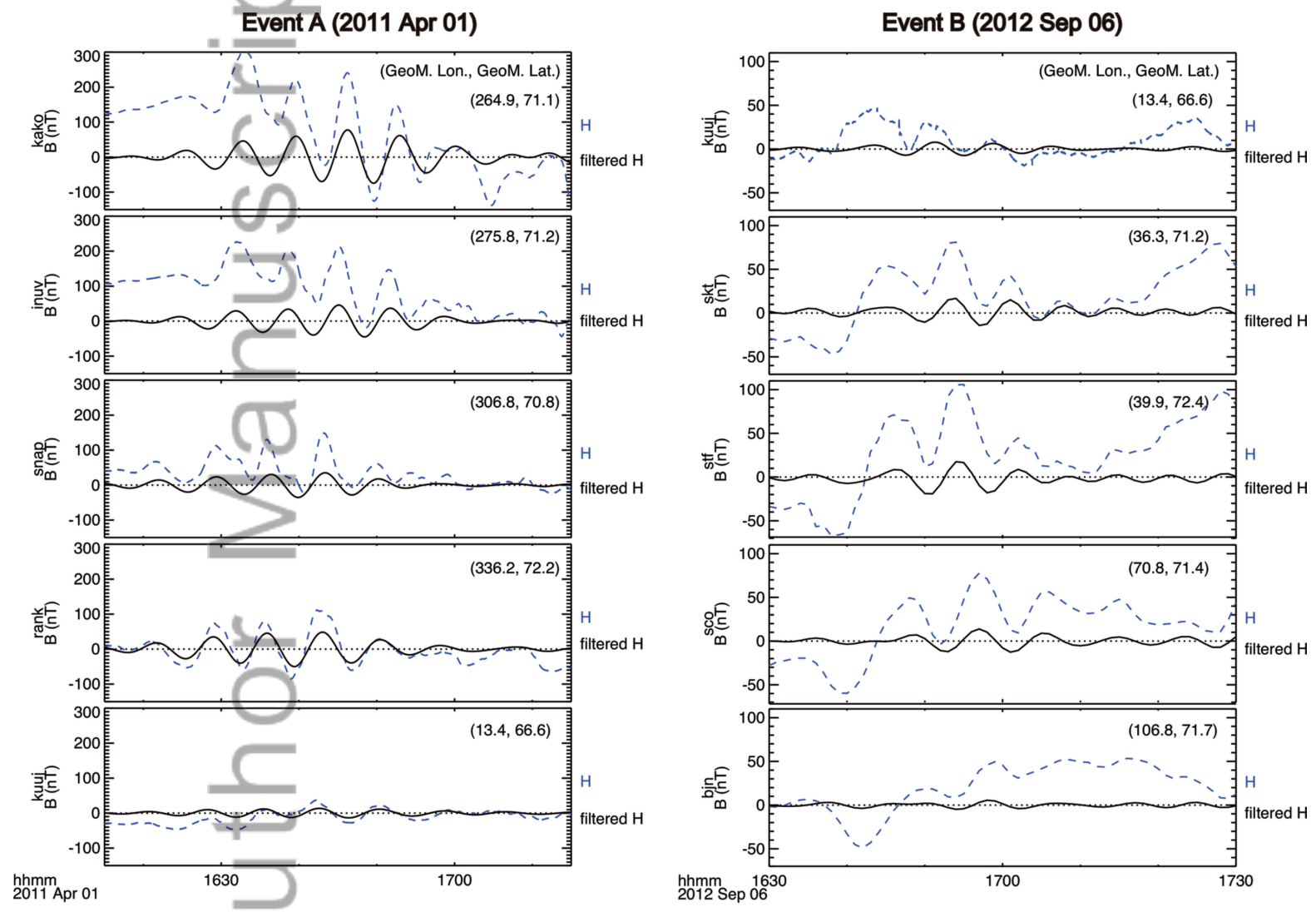

gmag_all

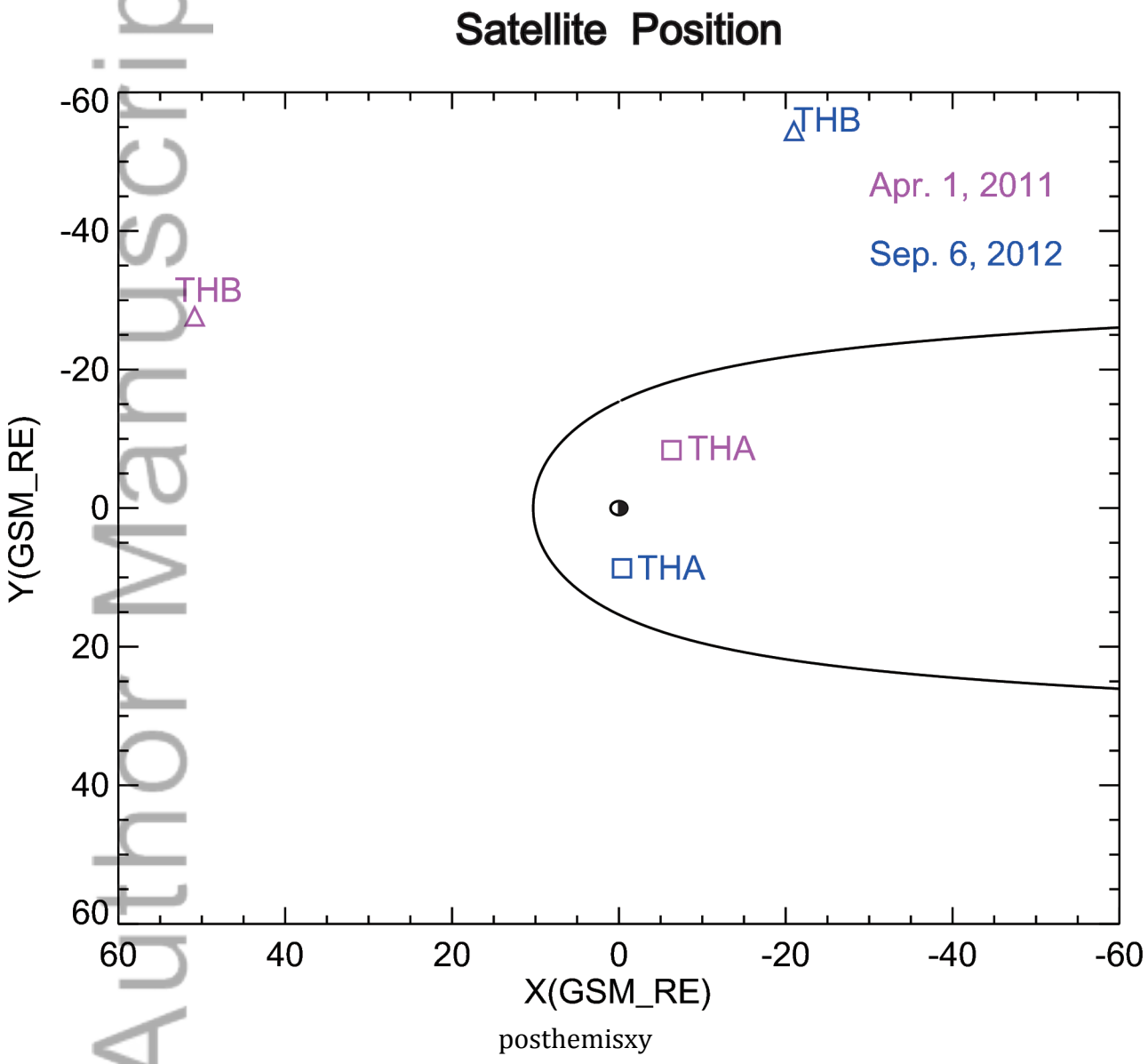

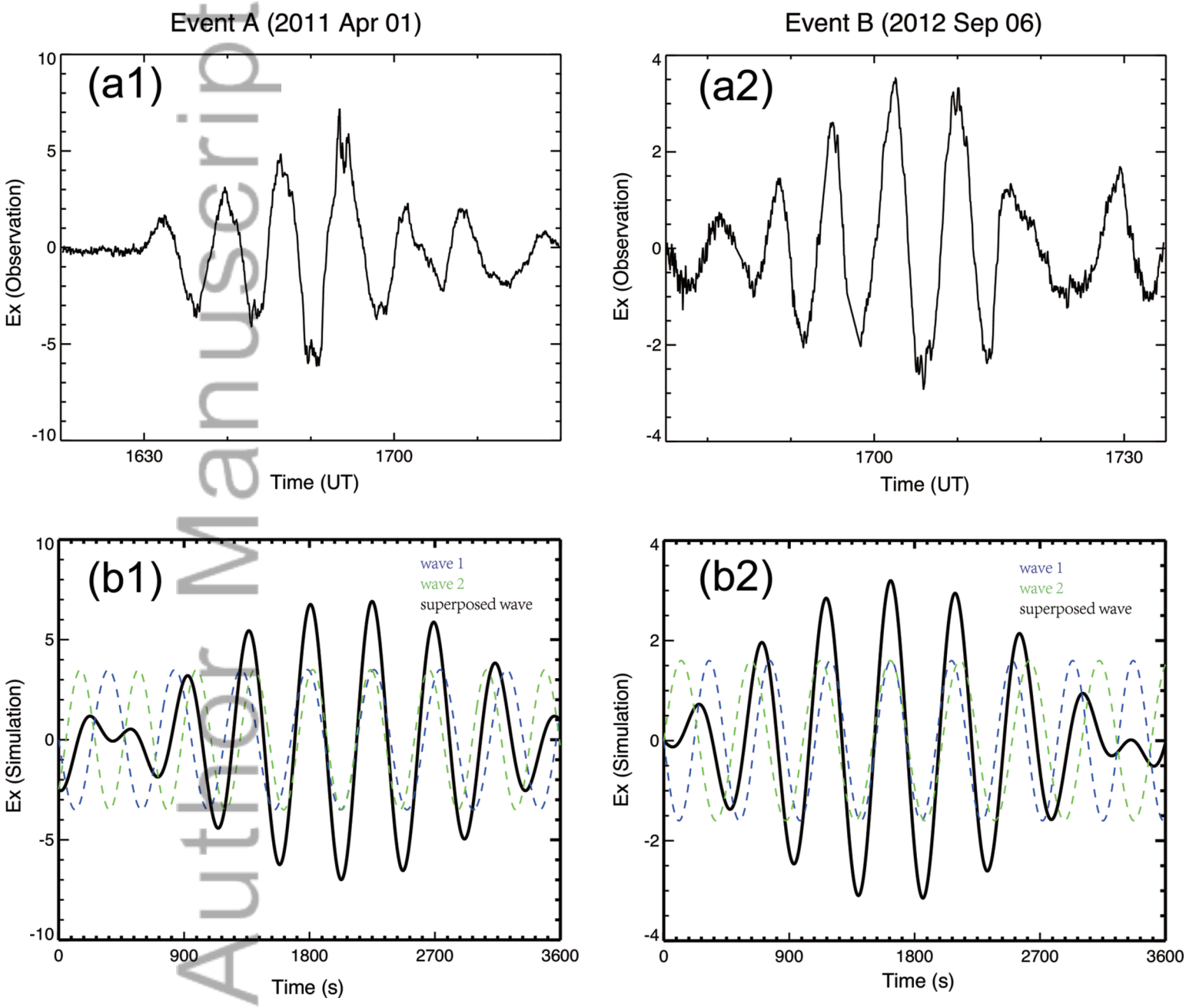

wave_diejia

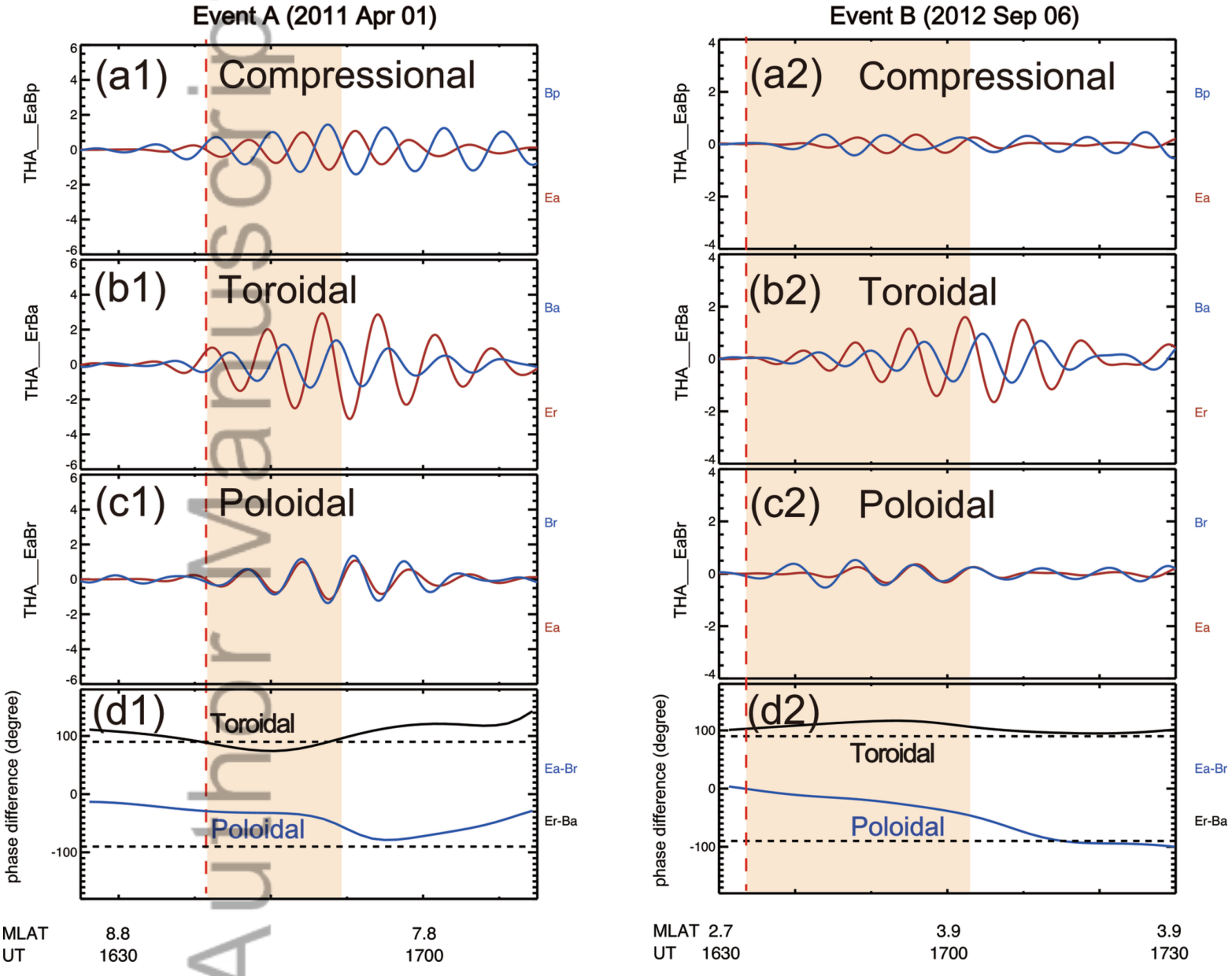

wave_mode_case

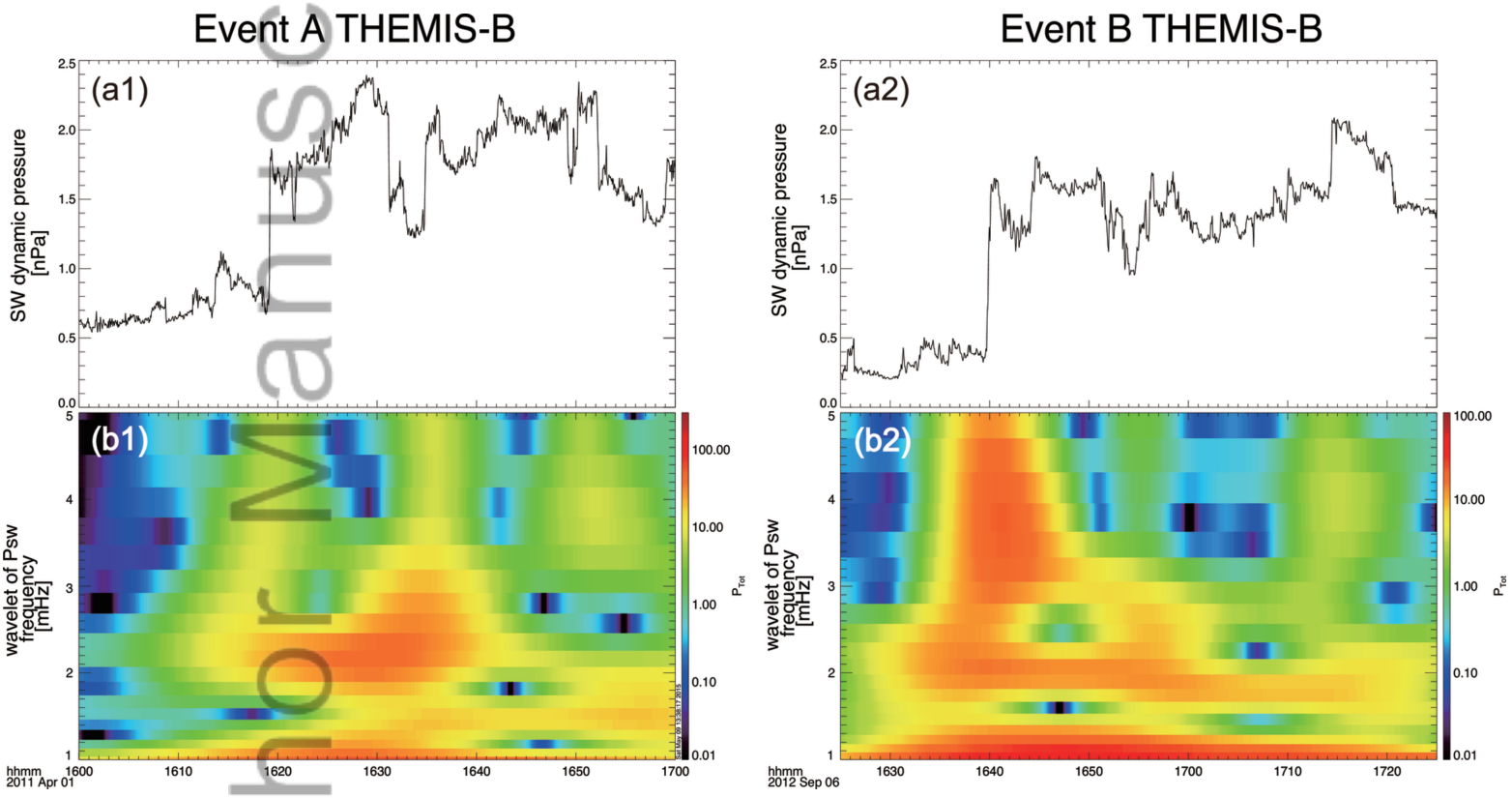

wavelet_psw

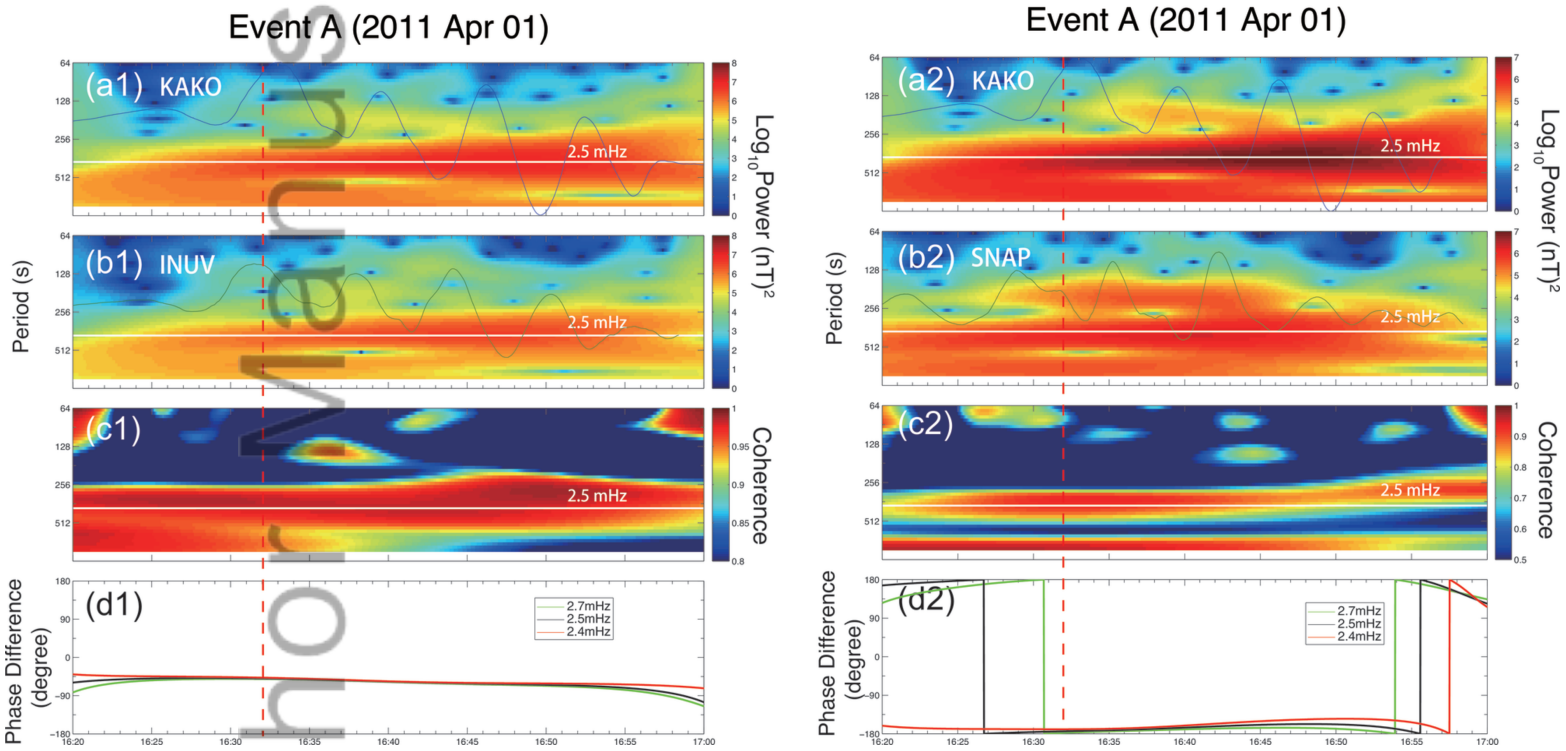

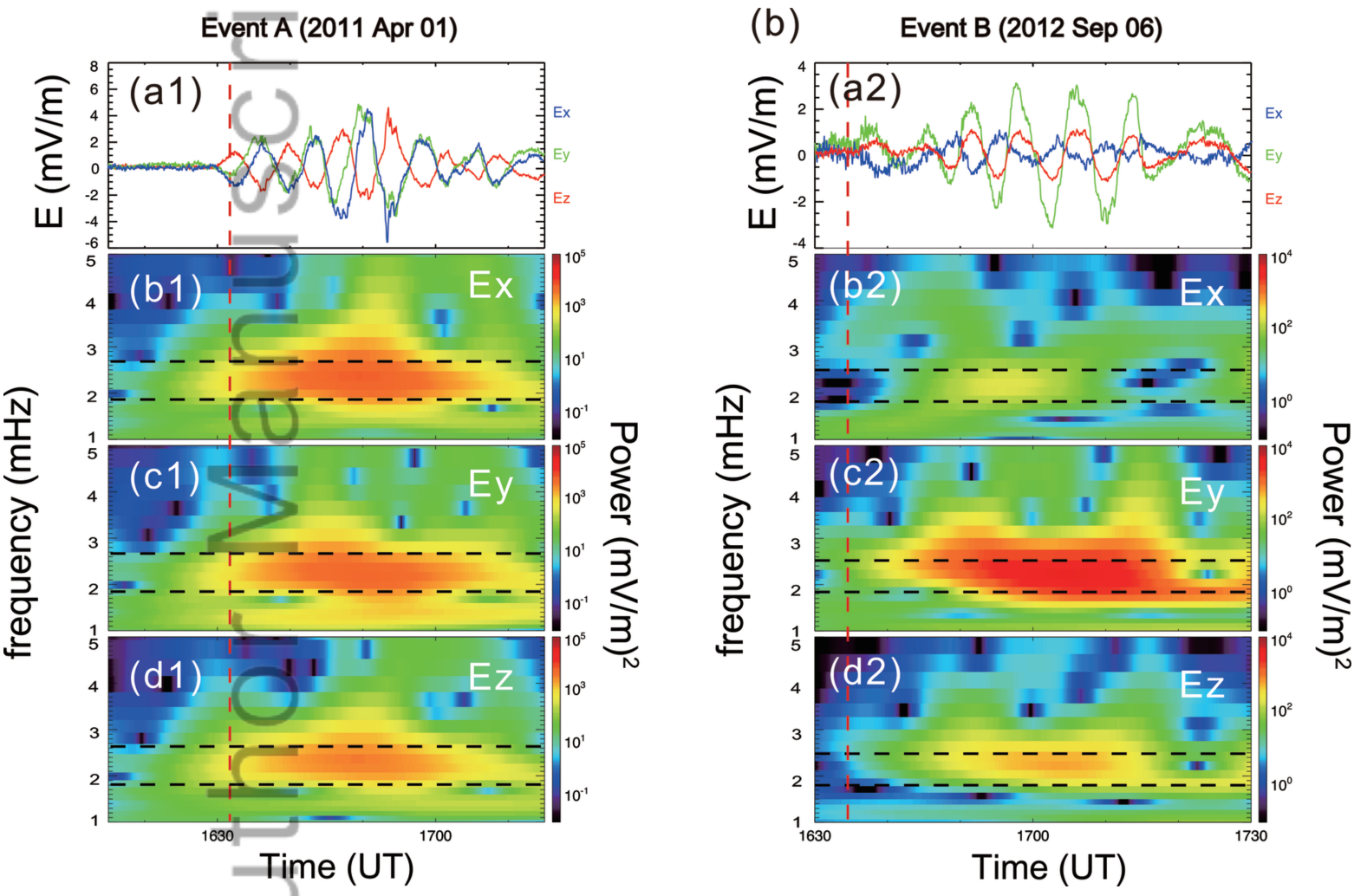

wvlt_tha_case

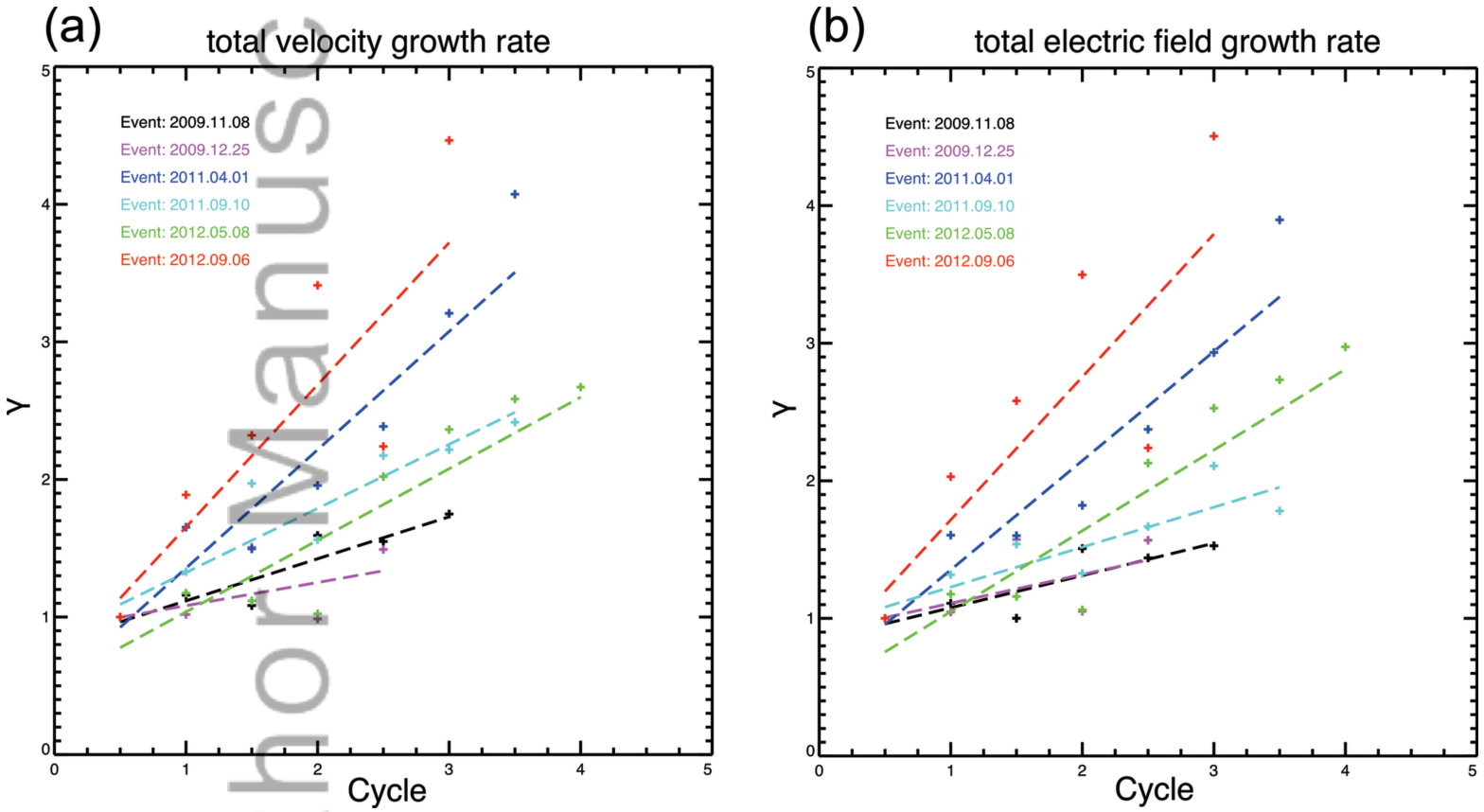

zzfd